




## New measures for analysis and comparison of shape distortion in world map projections

Melih Basaraner & Sinan Cetinkaya


To cite this article: Melih Basaraner & Sinan Cetinkaya (2019) New measures for analysis and comparison of shape distortion in world map projections, *Cartography and Geographic Information Science*, 46:6, 518-531, DOI: [10.1080/15230406.2019.1567394](https://doi.org/10.1080/15230406.2019.1567394)

To link to this article: <https://doi.org/10.1080/15230406.2019.1567394>

 View supplementary material 

 Published online: 04 Feb 2019.

 Submit your article to this journal 

 Article views: 327



 View related articles 

 View Crossmark data 

ARTICLE



# New measures for analysis and comparison of shape distortion in world map projections

Melih Basaraner  and Sinan Cetinkaya 

Division of Cartography, Department of Geomatic Engineering, Yildiz Technical University, Istanbul, Turkey

## ABSTRACT

World maps can have quite different depictions of reality depending on the projection adopted, and this can influence our perception of the world. In this respect, shape is a significant property that needs to be considered, especially when representing large regions in general-purpose world maps. A map projection distorts most geometric properties (area, distance, direction/angle, shape, and specific curves) and usually preserves a single property or provides a compromise between different properties when transforming terrestrial features from globe to plane. The distortions are mainly classified based on area, distance and direction/angle and analyzed with Tissot's theorem. However, this theorem offers a local (pointwise) solution, so the distortion assessment is valid at infinitesimal scale (i.e. for very small regions). For this reason, different approaches are required to analyze the distortions at finite scale (i.e. for larger regions). However, there are very few attempts at analyzing and comparing shape distortion of landmasses in world map projections owing to the fact that shape measurement is difficult and usually involves measuring different characteristics. Seeking to fill this gap, in this study, compactness and elongation distortion measures are introduced. In this regard, 16 world map projections are analyzed and compared with these distortion measures in a GIS environment, based on map datasets of continents and countries. An analysis of the effect of the levels of detail of the datasets is also presented.

## ARTICLE HISTORY

Received 26 December 2017  
Accepted 7 January 2019

## KEYWORDS

Shape distortion; world map projections; compactness distortion; elongation distortion; finite scale

## 1. Introduction

Distortions are an inevitable characteristic of every map projection. No map projection can preserve all geometric properties (area, distance, direction/angle, shape, and specific curves) at every location when projecting terrestrial features from globe to plane. For this reason, map projections are usually developed in a way so as to preserve a single property or to provide a compromise between different properties by permitting their slight distortions.

The fundamental approach used in the distortion analysis of a map projection is Tissot's theorem. Based on differential geometry, Tissot's theorem investigates the geometric relationships between a circle on the globe and its projection on the plane, called Tissot's indicatrix (the ellipse of distortion), at an infinitesimal scale. Thus, it enables calculating the distortions of the area, distance, direction/angle for map projections locally (i.e. pointwise). The problem of the Tissot's theorem is that it can solely be utilized for pointwise or local distortion analysis so this approach cannot be used directly for large terrestrial features of the world. Goldberg and Gott (2007) introduce new measures of

curvature distortions (flexion and skewness) that can be calculated at the finite scale. They also present a new graphical tool, called the Goldberg-Gott indicatrices, which can be used to show not only area and isotropy distortions but also flexion and skewness distortions in map projections. However, they do not consider the boundaries of the landmasses.

In map projections, the distortions of geometric properties are obtained by comparing their global (i.e. ellipsoidal or spherical) and planar magnitudes. Areas, distances, and angles/directions are the main geometric properties used for the evaluation of different map projections because they are easily measurable. On the other hand, as a geometric property, measuring the shape is non-trivial, even on the plane, because of its complex nature. The shape distortion can be defined as the variation occurring in the shape of terrestrial features when they are transformed from the globe to the plane. Since general-purpose world maps influence to a great extent our perception of the world, a good representation of shapes of the terrestrial features should be a major concern. When intended to show the shapes of terrestrial features with minimum distortions, conformal projections come to mind at first.

Conformal projections preserve the relative local angles about every point on the map. At the infinitesimal scale, the distortion of scale is equal in all directions and hence local shapes are preserved in conformal projections. In other words, an infinitesimal circle on the globe projects as a circle with a different radius on the plane (Canters, 2002; Snyder, 1987). Although conformal projections provide a good representation of shapes for a small area around every point, the rapid increase in the particular scales away from the points or lines of zero distortion make these projections less suitable for representing large terrestrial features like continents and oceans (Maling, 1992). To sum up, there is no clear information on how well conformal projections show the shapes of large terrestrial features whereas we know that they retain local shapes and exaggerate the sizes excessively away from the points or lines of zero distortion.

### 1.1. Related work

Shape distortion is investigated with visual and quantitative approaches in map projections. There are a very small number of studies that focus on shape distortion visualization for map projections. In this context, Brainerd and Pang (2001) introduce a software called the Interactive Map Projections system that can display both the globe and its corresponding representations in different map projections. Furthermore, their software can visualize the area and angular distortions by utilizing the circles that can interactively be drawn with arbitrary radii at different locations on the globe. Mulcahy and Clarke (2001) review various methods that can be used for symbolizing map projection distortion, including Tissot's indicatrix, the isoline (isocol) and the checkerboard among others. Some studies, described below, concentrate on quantifying shape distortion on map projections over large regions. There are mainly two approaches in this context. The first approach performs numerical integration of shape indicators based on Tissot's indicatrix at the points that fall within the regions. Kimerling, Overton, and White (1995) propose an approach for analyzing map projection distortions within irregular areas by calculating cumulative distribution functions and descriptive statistics of scale, angle, and shape distortions. In this context, they offer a new shape distortion measure calculated with Equation 1 at both regular and random sample points.

$$z = \sqrt{h^2 + k^2} - \sqrt{2} \quad (1)$$

where  $z$  is shape distortion measure,  $h$  is scale factor along the meridian,  $k$  is scale factor along the parallel.

The drawback of this method is that it is sensitive to the size. For example, it does not produce zero (no shape distortion) except for the standard lines where  $h = k = 1$  although the shape of infinitesimal circles on the globe is also preserved at the other locations where  $h = k > 1$  in conformal projections.

Laskowski (1997) extends the notion of distortion at a single point (point-distortion) to form the distortion measure for an arbitrarily large region. In his approach, the shape is measured with Equation 2 at selected points, based on Tissot's indicatrix. Then, regional shape distortion is calculated by the average of the square of individual contributions from a finite number of discrete points (spaced randomly or regularly) within a region (Equation 3). The main drawback of this method is that the shape distortion indicator will be zero at all points in conformal projections because the semi-axes of the indicatrix are equal and hence the mean-square shape distortion measure for a finite region will also be zero despite the fact that the shapes of large landmasses distort. In other words, the average of point-based distortions cannot reflect the actual shape distortions of the large landmasses sufficiently.

$$e_{shape} = \left( \frac{a}{b} - 1 \right) \quad (2)$$

$$\begin{aligned} E_{shape} &= \left( \frac{1}{N} \right) \sum_1^N e_{shape}^2 \\ &= \left( \frac{1}{N} \right) \sum_{i=1}^N \left( \frac{a_i}{b_i} - 1 \right)^2 \end{aligned} \quad (3)$$

where  $e_{shape}$  is shape distortion indicator,  $a$  is long axis of the indicatrix,  $b$  is the short axis of the indicatrix,  $E_{shape}$  is the mean-square shape distortion measure for a finite region.

The second approach produces a regional shape indicator to analyze shape distortions. Canters (2002) uses the shape analysis method proposed by Boyce and Clark (1964) to measure the shape distortions of spherical hexadecagons after they have been projected on to the plane. He chooses randomly distributed points over the landmasses and creates a multitude of hexadecagons with randomly changing radii (circular radius  $\leq 30^\circ$ ) at those points. When calculating Boyce and Clark's shape measure, the radial distances on the projection plane are calculated from the projected centroids of spherical hexadecagons instead of the centroids of the projected hexadecagons, which can influence the length of the radial lines and hence change the value of the measure slightly. In addition, he does not consider either physical or administrative boundaries directly. To be specific, he chooses the points falling within the continents but does not use the boundary geometry or geometric properties

of the polygons belonging to landmasses. Furthermore, the sizes (i.e. areas) of hexadecagons are not considered as weights when calculating the mean shape distortion of different map projections. Canters, Deknopper, and De Genst (2005) propose a method that numerically integrates shape and relative area distortions in a map projection to be used for producing compromise projections. In their study, the shape distortion of the hexadecagons falling within continental areas is again analyzed through Boyce and Clarke's radial shape analysis method. Their findings show that shape distortion is the highest in equal-area projections and the projections with low distortion of area. Their analysis again has the same weakness mentioned above.

### 1.2. Motivation and objectives

Very few attempts have so far been made to analyze and compare shape distortions in world map projections at the finite scale due to the fact that shape is not easy to define (Canters, 2002; Robinson & The Committee on Map Projections, 2017). Previous methods have two key problems. First, they do not use the geometric properties of the fiat and bona fide boundaries in the analysis. Second, most of them are based on the infinitesimal scale calculations that cannot reflect the distortions at the finite scale effectively. Therefore, this study aims at developing a practical and useful approach to analyze and compare the shape distortions of large landmasses (continents and countries) in world map projections. In this respect, two new measures (indices) are introduced that function directly at the finite scale and then employed individually for the analysis and comparison of shape distortion in 16 world map projections within a GIS environment.

## 2. A brief overview of shape analysis

Perception of shapes is relatively easy for humans, but it is fairly complicated to achieve this computationally. Shape measures usually analyze only one characteristic of shape and produce a single value. When considering the variety of shapes, it is difficult for a single value to represent such variety in a sufficiently effective way. Therefore, the performance of these methods tends to decrease as the shape complexity increases. The collective use of the measures may be considered in this context (Basaraner & Cetinkaya, 2017).

There is a wide range of shape analysis methods in the fields of geography, pattern recognition, cartography and GIScience. A good overview of the subject can be found in MacEachren (1985), Wentz (1997), Costa

and Cesar (2009), Angel, Parent, and Civco (2010) and Neal and Russ (2012). One of the most common methods employed for measuring the shape of a polygon is to calculate its compactness. A circle is considered to be the most compact shape so the compactness measures find the deviation of a polygon from a circle. This is generally carried out based on either the lengths of the radial lines between the boundary points and the centroid of a polygon, as in Boyce and Clark's method, or the ratio of the area of a polygon to the area of the equal-perimeter circle. Different formulations of compactness exist, mainly using these two approaches or their variations (Angel et al., 2010; MacEachren, 1985). Other commonly used shape measures include rectangularity, convexity, and elongation (eccentricity) (Basaraner & Cetinkaya, 2017; Neal & Russ, 2012). Rectangularity finds the areal deviation of a polygon from its minimum area bounding rectangle. Convexity or concavity finds the areal deviation of a polygon from its convex hull. Eccentricity or elongation finds the ratio of minimum and major axes of a polygon.

## 3. New measures for shape distortion analysis at the finite scale

Shape distortion analysis in map projections requires the measurement of the shape characteristics both on the globe and the projection plane at the finite scale. In this regard, one of the main challenges is to identify suitable planar methods that can be adapted to the globe. Another critical point is that these methods should be sufficiently sensitive to the distortion.

Since the world maps are produced at very small scales (typically smaller than 1:20 000 000), we can use the sphere as a reference surface instead of the ellipsoid for the globe due to the fact that the differences become less than the geometric accuracy requirements of world maps. Thus, the calculations can be made easier.

Although there are many methods for measuring shapes of planar polygons, no method is available that works on the sphere for arbitrary polygons according to our knowledge. In this context, spherical versions of two shape measures (i.e. compactness and elongation) were developed and thus new compactness and elongation distortion measures were introduced as the shape distortion measures for world map projections. Among the existing shape measures, these two have been chosen because they are widely used in shape analysis (Angel et al., 2010; Neal & Russ, 2012). In addition, their underlying approaches are more practical to adapt to the sphere.

### 3.1. Compactness distortion and distortion indicator

Compactness (also known as circularity) of a polygon is often measured with the different formulations based on its area and perimeter. Several versions of these formulations can be found in the related literature (Angel et al., 2010; Basaraner & Cetinkaya, 2017; Costa & Cesar, 2009; MacEachren, 1985; Neal & Russ, 2012). In a practical sense, to derive the compactness formulation, the area of a polygon is divided by the square of the perimeter of the polygon and this ratio is then multiplied by a coefficient so that its value becomes equal to 1 for a circle. For the distortion calculation, both planar and spherical compactness of the polygons have to be obtained.

The planar compactness is formulated in two steps. In the first step, the coefficient is calculated by dividing the square of the perimeter of a planar circle by its area (Equation 4). In the second step, the polygon's area is divided by the square of its perimeter and this ratio is then multiplied by the coefficient (Equation 5). The compactness decreases as both the shape complexity of the landmasses (i.e. departing from simple and regular shapes) and the amount of intrusions and protrusions along their boundary increase.

$$k_{pl} = \frac{P_{pl,c}^2}{A_{pl,c}} = \frac{(2\pi r)^2}{\pi r^2} = 4\pi \quad (4)$$

$$C_{pl} = k_{pl} \frac{A_{pl}}{P_{pl}^2} = 4\pi \frac{A_{pl}}{P_{pl}^2} \quad (5)$$

where  $k_{pl}$  is the coefficient for planar polygons,  $A_{pl,c}$ ,  $P_{pl,c}$  and  $A_{pl}$ ,  $P_{pl}$  are, respectively, the area and the perimeter of a planar circle and a planar polygon,  $r$  is the radius of the circle,  $C_{pl}$  is the planar compactness of a polygon.

The spherical compactness is formulated in three steps. First, the spherical cap angle (see Figure 1) is calculated based on the equal-area spherical circle (i.e. spherical cap) of a spherical polygon (Equation 6). Then, the coefficient is calculated by dividing the square of the perimeter of a spherical circle by its area (Equation 7). Finally, the polygon's area is divided by the square of its perimeter and this ratio is then multiplied by the coefficient (Equation 8). As stated above, the compactness of a spherical circle is equal to 1. This value decreases with lessening compactness of a polygon. Here, if the cap angle is calculated based on the equal-perimeter circle of the polygon, it becomes undefined for the large landmasses with very irregular boundaries since their perimeters are greater than the perimeter of the sphere.

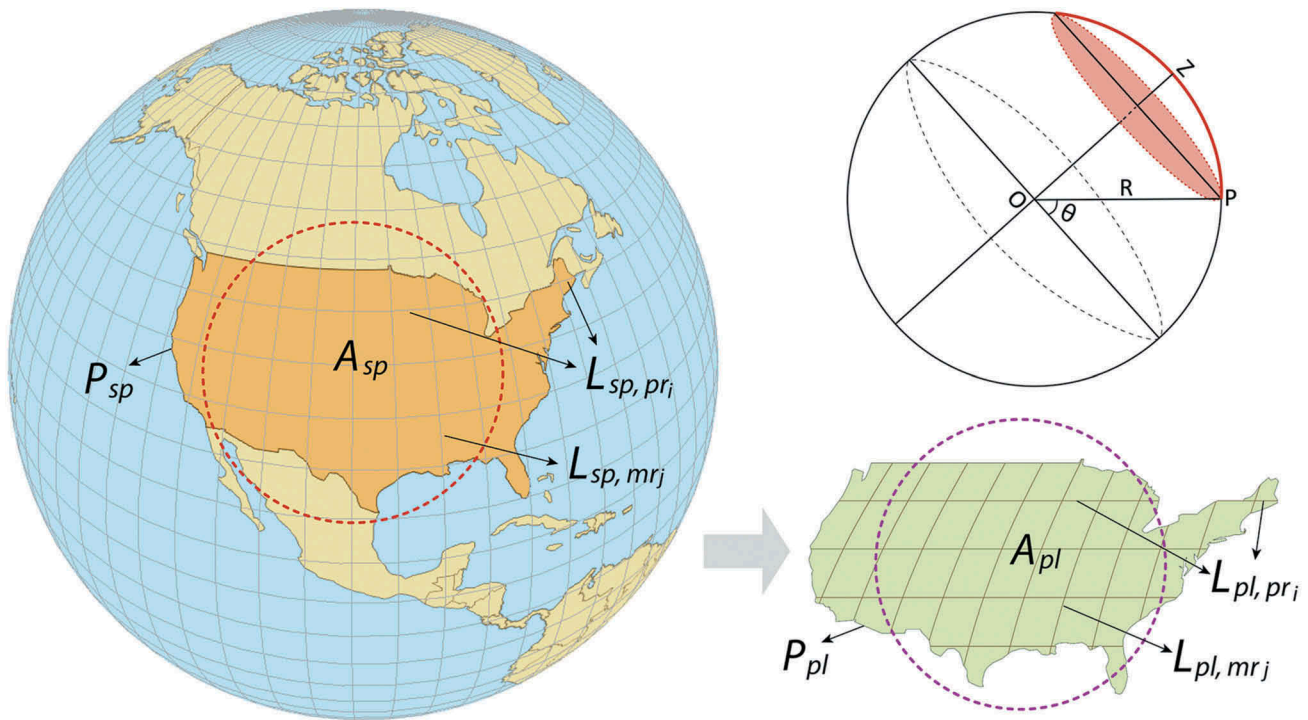


**Figure 1.** The geometric elements used in the equations of compactness and elongation distortions. See the equations in Sections 3.1 and 3.2 for the meaning of the symbols.



$$\theta = \sin^{-1} \left( 1 - \frac{A_{sp}}{2\pi R^2} \right) \quad (6)$$

$$k_{sp} = \frac{P_{sp,c}^2}{A_{sp,c}} = \frac{(2\pi R \cos \theta)^2}{2\pi R^2 (1 - \sin \theta)} = 2\pi (1 + \sin \theta) \quad (7)$$

$$C_{sp} = k_{sp} \frac{A_{sp}}{P_{sp}^2} = 2\pi (1 + \sin \theta) \frac{A_{sp}}{P_{sp}^2} \quad (8)$$

where  $\theta$  is the spherical cap angle,  $R$  is the radius of the sphere (i.e. 6371 km),  $A_{sp,c}$ ,  $P_{sp,c}$  and  $A_{sp}$ ,  $P_{sp}$  are, respectively, the area and the perimeter of a spherical

circle and a spherical polygon,  $k_{sp}$  is the coefficient for spherical polygons,  $C_{sp}$  is the spherical compactness of a polygon.

Some examples of the spherical and planar compactness measures are given in Figure 2. When the appearances of the landmasses are examined, it can be seen that their compactness values reflect the shape variations induced from map projections fairly well. For example, when looking at Greenland, the greatest variation is perceived in Plate Carree while the least variation is observed in Mercator in parallel to the changes in their compactness values.

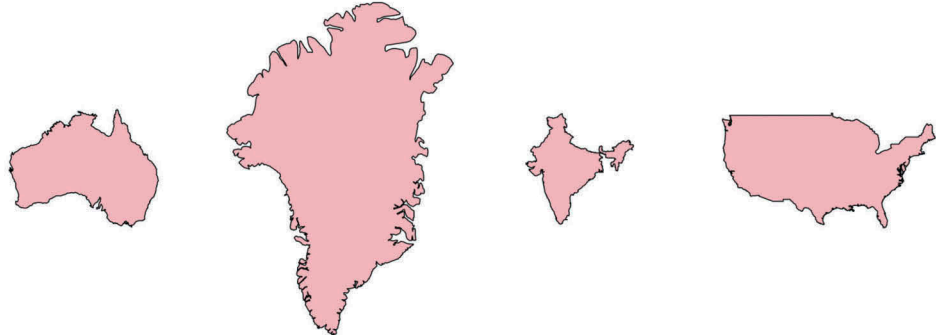



SPHERE	COMsp	0.286	0.096	0.155	0.184
	ELOsp	1.274	0.671	0.979	1.847
MERCATOR					
	COMpl	0.290 ↑	0.104 ↑	0.153 ↓	0.191 ↑
	ELOpl	1.270 ↓	0.596 ↓	0.978 ↓	1.835 ↓
					
PLATE CARREE	COMpl	0.290 ↑	0.053 ↓	0.154 ↓	0.179 ↓
	ELOpl	1.420 ↑	2.563 ↑	1.068 ↑	2.403 ↑
MOLLWEIDE					
	COMpl	0.247 ↓	0.068 ↓	0.148 ↓	0.169 ↓
	ELOpl	0.974 ↓	0.994 ↑	0.812 ↓	1.498 ↓
					
ROBINSON	COMpl	0.275 ↓	0.062 ↓	0.153 ↓	0.182 ↓
	ELOpl	1.163 ↓	1.804 ↑	0.910 ↓	1.823 ↓

Figure 2. Spherical and planar compactness and elongation values of sample landmasses in some map projections. Up arrow (↑) and down arrow (↓) respectively, show increasing and decreasing values.

The compactness distortion of a polygon is calculated by dividing its planar compactness by its spherical compactness (Equation 9). Accordingly, one of three different cases can arise for a polygon's compactness after projection: it decreases if  $C_{dst} < 1$ , increases if  $C_{dst} > 1$  and does not change if  $C_{dst} = 1$ . Since  $C_{dst}$  can be greater or less than 1, it needs to be standardized in a proper way to find the correct amount of distortion irrespective of the increase or the decrease of  $C_{dst}$ . Therefore, the compactness distortion indicator is formulated in a way so as to produce values between 0 and 1 (Equation 10). This is done first by applying a minimum function to the distortion and the inverse of the distortion values to constraint them to be at most 1 and then by subtracting the resulting value from 1. Thus, the value of zero corresponds to no distortion. In fact,  $\Delta C_{dst}$  never becomes 0 for the landmasses if it is computed with enough precision because world map projections distort their shapes, albeit to a minor extent for some of them, and never becomes 1 since  $C_{dst}$  is always greater than zero.

$$C_{dst} = \frac{C_{pl}}{C_{sp}} = \frac{2A_{pl}P_{sp}^2}{(1 + \sin\theta)A_{sp}P_{pl}^2} \quad (9)$$

$$\Delta C_{dst} = 1 - \min\left(C_{dst}, \frac{1}{C_{dst}}\right) \quad (10)$$

where  $C_{dst}$  is the compactness distortion of a landmass polygon and  $\Delta C_{dst}$  is the compactness distortion indicator of a landmass polygon.

### 3.2. Elongation distortion and distortion indicator

The elongation of a polygon on the plane is usually calculated with the ratio of the axes of the minimum area bounding rectangle of the polygon. However, it is not easy to adapt this approach to the polygons on the sphere. Therefore, in this study, a more practical measure is proposed for the elongation that works based on the graticule (Figure 1). To be specific, the ratio of the average length of the parallel line sections to the average length of the meridian line sections falling within each landmass is computed both on the plane and the sphere to find planar and spherical elongation, respectively (Equations 11 and 12).

$$E_{pl} = \frac{\frac{1}{n_{pr}} \sum_{i=1}^{n_{pr}} L_{pl, pr_i}}{\frac{1}{n_{mr}} \sum_{j=1}^{n_{mr}} L_{pl, mr_j}} \quad (11)$$

$$E_{sp} = \frac{\frac{1}{n_{pr}} \sum_{i=1}^{n_{pr}} L_{sp, pr_i}}{\frac{1}{n_{mr}} \sum_{j=1}^{n_{mr}} L_{sp, mr_j}} = \frac{\frac{1}{n_{pr}} \sum_{i=1}^{n_{pr}} R \cos \varphi_i (\lambda_{e,i} - \lambda_{s,i})}{\frac{1}{n_{mr}} \sum_{j=1}^{n_{mr}} R (\varphi_{e,j} - \varphi_{s,j})} \quad (12)$$

where  $E_{pl}$  and  $E_{sp}$  are, respectively, planar and spherical elongation,  $L_{pl, pr}$ ,  $L_{pl, mr}$ ,  $L_{sp, pr}$  and  $L_{sp, mr}$  are the lengths of parallel and meridian line sections on the plane and the sphere,  $n_{pr}$  and  $n_{mr}$  are, respectively, the numbers of parallel and meridian line sections of different latitudes and longitudes,  $\lambda_s$ ,  $\varphi_s$ , and  $\lambda_e$ ,  $\varphi_e$  are, respectively, the geographic coordinates of the start and the end points of the line sections (in radians),  $i$  and  $j$  are, respectively, the indices for the parallel and meridian sections.

Some examples of spherical and planar elongation measures are given in Figure 2. When the appearances of the landmasses are examined, it can be seen that their elongation values reflect the shape variations induced from map projections quite well. For example, when looking at Australia, the greatest variation is perceived in Mollweide while the least variation is observed in Mercator in parallel to the changes in their elongation values.

The elongation distortion of a polygon is calculated by dividing its planar elongation by its spherical elongation (Equation 13). Accordingly, one of three different cases can arise for a polygon's elongation after projection: it decreases if  $E_{dst} < 1$ , increases if  $E_{dst} > 1$  and does not change if  $E_{dst} = 1$ . The elongation distortion indicator is formulated in such a way as to produce values between 0 and 1 by using the same procedure as applied to  $\Delta C_{dst}$  (Equation 14) and hence both carry the same properties (mentioned in Section 3.1).

$$E_{dst} = \frac{E_{pl}}{E_{sp}} \quad (13)$$

$$\Delta E_{dst} = 1 - \min\left(E_{dst}, \frac{1}{E_{dst}}\right) \quad (14)$$

where  $E_{dst}$  is the elongation distortion of a landmass polygon and  $\Delta E_{dst}$  is the elongation distortion indicator of a landmass polygon.

### 3.3. Mean distortion indicators for world map projections

The mean distortion value of each indicator is found by calculating the weighted average of their landmass-based values to compare world map projections in terms of shape distortion (Equation 16). Since the landmasses have different sizes, their spherical areas are

used as weights in the calculation of the mean distortion indicator for each map projection.

$$\bar{I} = \frac{\sum_{u=1}^{n_{lm}} A_{sp_u} I_u}{\sum_{u=1}^{n_{lm}} A_{sp_u}} \quad (16)$$

where  $I$  is the distortion indicator (i.e.  $\Delta C_{dst}$  or  $\Delta E_{dst}$ ) of a landmass polygon,  $A_{sp}$  is the spherical area of a landmass polygon,  $u$  is the index of a landmass polygon,  $n_{lm}$  is the number of landmass polygons and  $\bar{I}$  is the mean distortion indicator of a map projection.

## 4. Experimental study

The experimental study includes continental and country-specific shape distortion analyses on the basis of map projection. These analyses were, respectively, performed with the compactness and elongation distortion indicators. In addition, the country-specific distortion analysis was repeated by employing two extra scales to investigate whether the level of detail (scale) had any meaningful effect on the distortion indicator values. Furthermore, a correlation analysis was carried out to understand the relationship between the indicators using Karl Pearson's coefficient of correlation (Ram, 2012). Additional explanations about the experimental study (i.e. data and implementation details) are given below.

### 4.1. Data

Four different datasets were used in the experimental study. These were open world map datasets showing continents and countries in the Geographic (WGS84) coordinate system. The first dataset was about the continents and obtained from the UCLA Geoportal ([http://gis.ucla.edu/geodata/dataset/continent\\_ln](http://gis.ucla.edu/geodata/dataset/continent_ln)). It was slightly modified

before its use since the boundaries of some continents were partly incorrect. There was no information about its scale or resolution but it had a higher level of detail than the second dataset that we used. The second dataset was obtained from the Natural Earth website (<http://www.naturalearthdata.com/downloads>). It was about the countries at the scale 1:50 000 000 (1:50 M). Additionally, again from the same website, two datasets about the countries at the scales 1:10 000 000 (1:10 M) and 1:110 000 000 (1:110 M) were used for analyzing the effect of the level of detail.

## 4.2. Implementation details

In total, 16 sphere-based world map projections were analyzed with respect to the shape distortions of the continents and countries. They were categorized with the distortion characteristics (i.e. Conformal, Equidistant, Equal-area, and Compromise) and briefly described in [Table 1](#). In the selection process, commonly used world map projections (Jenny, Savric, Arnold, Marston, & Preppernau, 2017; Savric, Jenny, White, & Strebe, 2015; Snyder, 1987) as well as those with the distinctive distortion patterns (i.e. Equidistant Secant Cylindrical, Bonne, and Polyconic) were selected to enable broader comparison. The default projection parameters offered by the software were used for obtaining the world maps. However, it should be noted that the default parameters may not always be the best option from the distortion aspect.

In the experimental study, ESRI ArcGIS<sup>TM</sup> ArcMap 10.4.1 software was used since it supports a wide range of sphere-based world map projections.

Since Antarctica contains the South Pole, it is represented as interrupted and hence severely distorted in many world map projections, particularly in those

**Table 1.** The world map projections used in the experimental tests (ESRI, 2004; Snyder, 1987).

[illegible]



representing the poles as lines or curves. Therefore, it was excluded from the analysis.

All polygons representing the continents, the countries or their disjoint parts such as islands and other discrete landmasses were analyzed individually. For example, contiguous U.S. and Alaska were dealt with as separate parts.

In the continental analysis, only very large landmasses (namely, the mainlands of the continents as well as Greenland) were used. For the country-specific analysis, the landmasses smaller than 62 500 km<sup>2</sup> on the sphere, which corresponds to 25 mm<sup>2</sup> in an equal-area map projection at the scale 1:50 M, were excluded from the dataset because they are very small and hence barely discernable. Consequently, 144 landmasses were analyzed. In the scale-based analysis, the compactness and elongation indicator values of the landmasses at 1:10 M, 1:50 M, and 1:110 M scales from the country-specific datasets were compared to each other.

The computations of the spherical and planar lengths and areas, as well as the distortions, were mainly performed with some simple Python functions and expressions as well as the relevant tools in the GIS software. To compute the elongation distortion, a graticule was created for the whole world with 0.5° intervals in Geographic (WGS84) coordinate system, in which both parallels and meridians were straight lines, and used for all of the map datasets. New vertices were interpolated on the graticule with 0.001° intervals before being transformed into a sphere-based map projection system. This is important for more smooth representation of the graticule geometry and thus performing a more precise length computation because the parallels and meridians are often represented with curves in many world map projections.

The specific steps for computing the elongation distortion in the GIS software are as follows:

- (1) Create the graticule with the determined interval,
- (2) Overlay the graticule with the landmass polygons and obtain parallel and meridian line sections within each polygon,
- (3) Compute the number of parallel and meridian line sections within the polygon,
- (4) Fragment these line sections if they are multi-part lines,
- (5) Compute their spherical lengths,
- (6) Compute the spherical elongation of each polygon with the ratio of the average spherical length of the parallel line sections to the average spherical length of the meridian line sections,

- (7) Densify the line sections with the determined interval (add extra vertices along the graticule lines),
- (8) Set a new map projection,
- (9) Compute the planar lengths of parallel and meridian line sections within each polygon,
- (10) Compute the planar elongation of each polygon with the ratio of the average planar length of the parallel line sections to the average length of the meridian line sections,
- (11) Compute the elongation distortion with the ratio of the planar elongation to the spherical elongation for each polygon.
- (12) Compute the distortion indicators for the landmass polygons.
- (13) Compute the mean distortion indicators.

In this process, steps (1)–(7) are performed once while the remaining steps are repeated for each map projection.

## 5. Results

This section presents the results of the continental and country-specific distortion analysis, the level of detail analysis and the correlation analysis.

### 5.1. Continental distortion analysis results

In the continental analysis, concerning the compactness distortion, the compromise projections yielded the lowest distortions, except for Polyconic. Mercator as a conformal projection also exhibited very similar performance. The equal-area projections usually produced the highest distortions. The lowest compactness distortion was produced by Times while the highest was produced by Cylindrical Equal-Area (Figure 3(a)).

Concerning the elongation distortion, Mercator and most of the Compromise projections yielded the lowest distortions. The Equal-area projections usually produced moderate or high distortions, but the distortion of Bonne was quite low. The Equidistant projections yielded quite high distortions. Polyconic had also a similar amount of distortion with them. The lowest elongation distortion was produced by Mercator while the highest was produced by Cylindrical Equal-Area (Figure 3(b)).

The continental distortion maps are presented in Appendices I and II (see Supplementary Materials). Two examples about the continents, including their appearances and distortion indicator values, are given in Appendix III (see Supplementary Materials).



**Figure 3.** Mean values of the compactness (a and c) and elongation (b and d) distortion indicators of continents and countries in the world map projections (in ascending order).

## 5.2. Country-specific distortion analysis results

In the country-specific analysis, concerning the compactness distortion, Mercator and most of the compromise projections yielded the lowest distortions. Plate Carree had also a similar amount of distortion to these. The equal-area projections produced the highest distortions. The lowest compactness distortion was produced by Times while the highest was produced by Sinusoidal (Figure 3(c)).

Concerning the elongation distortion, Mercator produced very low distortion. Bonne, as an equal-area projection, yielded low distortion, while the rest of the equal-area projections had moderate or high distortions. The compromise projections yielded quite low distortions, except for Polyconic. The lowest shape distortion was produced by

Mercator while the highest was produced by Equidistant Secant Cylindrical (Figure 3(d)).

The country-specific distortion maps are presented in Appendices IV and V (see Supplementary Materials). Figure 4 shows the appearances and distortion indicator values of Australia (mainland) for each map projection. Other examples about the countries are given in Appendix VI (see Supplementary Materials).

## 5.3. Analysis of the effect of the level of detail

In this phase, the compactness and elongation indicator values were analyzed with respect to the level of detail

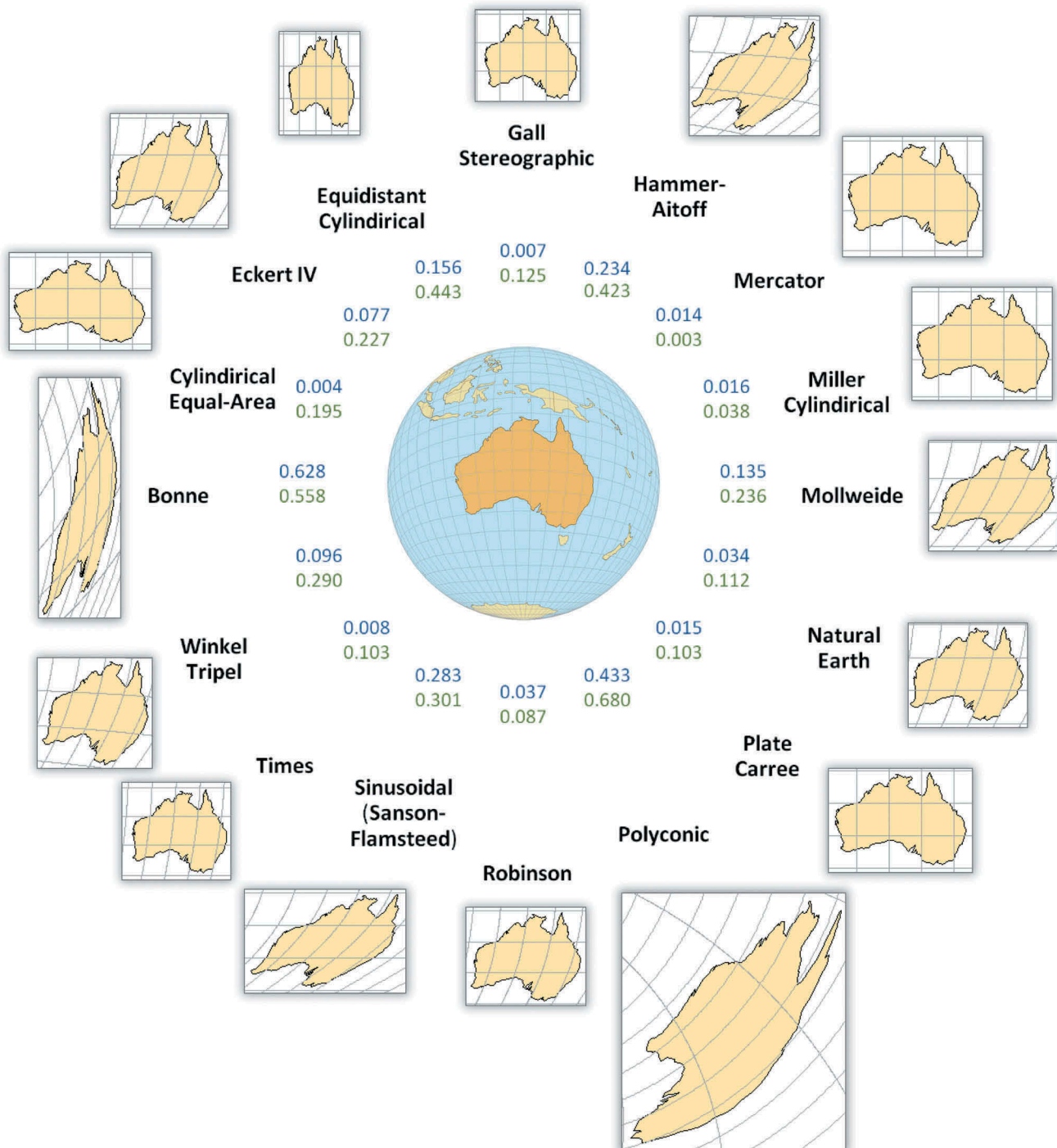


**Figure 4.** The values of compactness (blue) and elongation (green) distortion indicators of Australia (mainland).

variation using the landmass polygons at three different scales (i.e. 1:10 M, 1:50 M, and 1:110 M) based on the map projections and the results about the largest 12 landmasses were shown in Appendix VII (see Supplementary Materials). Accordingly, the effect of the level of detail was low or moderate except for the landmasses with very irregular boundary (e.g. Canada, Greenland, and Russia) for the compactness distortion

indicator. On the other hand, it was very low for the elongation distortion indicator.

#### 5.4. Correlation between the distortion indicators

The correlations between the compactness and elongation distortion indicators were computed through the country-specific dataset. Their correlations varied

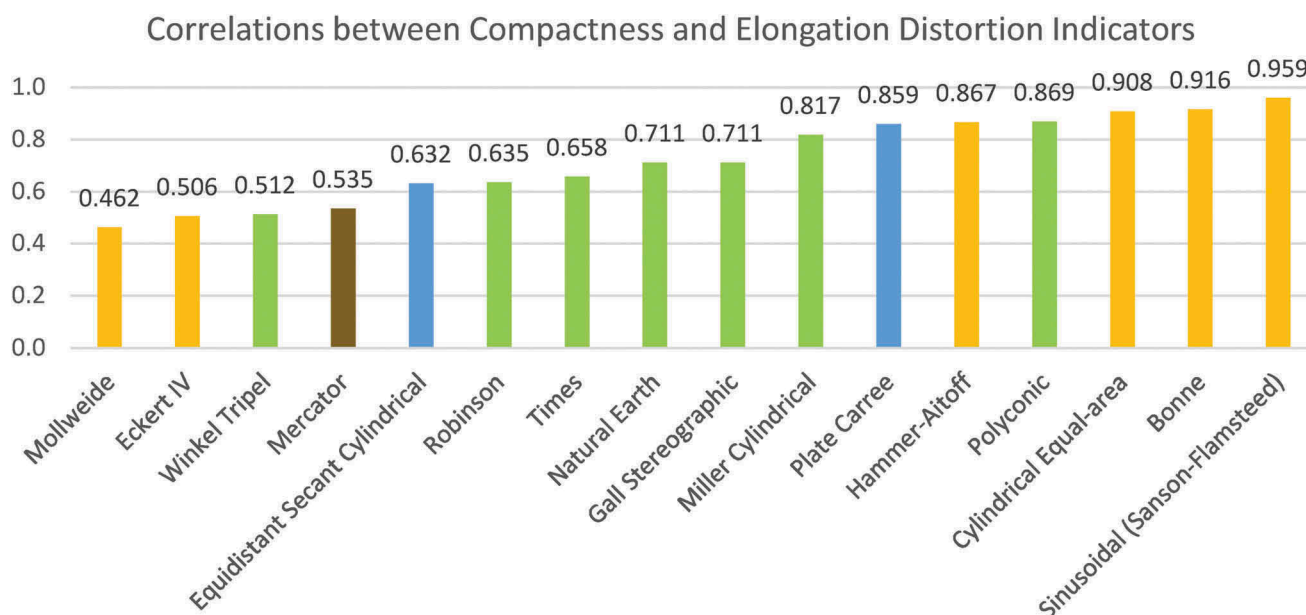


**Figure 5.** Correlations between the compactness and elongation distortion indicators in the world map projections (in ascending order).

depending on the map projections (Figure 5). The highest correlation was produced by Sinusoidal (Sanson-Flamsteed) at 0.959, while the lowest correlation was produced by Mollweide at 0.462.

## 6. Discussion

The map projections that were tested produced different amounts of distortions for the landmasses. As can be seen from the maps given in Appendices I, II, IV, and V, the shape distortions increase proportionally as the distance from the lines or points of zero distortion increases. In the orthogonal projections, where the parallels and meridians intersect at right angles, such as Mercator and Plate Carree, the shape distortion mainly depends on latitude and increases as the distance from standard parallel(s) increases while in the non-orthogonal projections such as Robinson and Winkel Tripel, it depends on both latitude and longitude, and increases as the distance from standard parallel(s) and central meridian increase. Another factor that affects the shape distortions of the landmasses is the spread of their spatial extents over the earth since they are polygonal. The effect of the spread can more easily be understood if the distortions are examined pointwise over a landmass.

Furthermore, the specific characteristics of the indicators can influence the distortion values in some amount. For the compactness distortion indicator, the scale distortions can change along the boundaries of the landmasses. To be specific, the scale distortions of the boundary segments depend on their directions (except for very short

segments on Mercator since it is a conformal projection). This changes the perimeter of a landmass polygon more than its area and hence affects the indicator value. An example of this is Madagascar (relative to its neighbors) in Bonne, Equidistant Secant Cylindrical and Eckert IV as shown in Appendix IV. For the elongation distortion indicator, there may be a difference between orthogonal and non-orthogonal projections with respect to scale distortion. According to Tissot's theorem, the directions of maximum and minimum scale distortions coincide with the graticule in orthogonal projections while they partly deviate from the graticule in non-orthogonal projections. Although its impact at the finite scale is not obvious, this may affect the values of the elongation distortion indicators of the landmasses. To be specific, in the first case, the indicators are computed from the maximum and minimum scale distortion values (i.e. extreme values) while in the second case, these values may differ from the extreme values in some amount, which can cause partly smaller indicator values, since the graticule does not correspond to the directions of extreme scale distortions.

As shown in Appendices I–VI, the compactness and elongation distortion indicators usually responded well to the shape distortions induced by map projections. One of the evidence of this is that Mercator, as a conformal projection, yielded rather low distortions as expected. The correlations between the indicators show that they usually have a similar response to the shape distortion although the amount of the similarity changes depending on the map projection.

The elongation distortion indicator usually yielded higher values than the compactness distortion indicator,



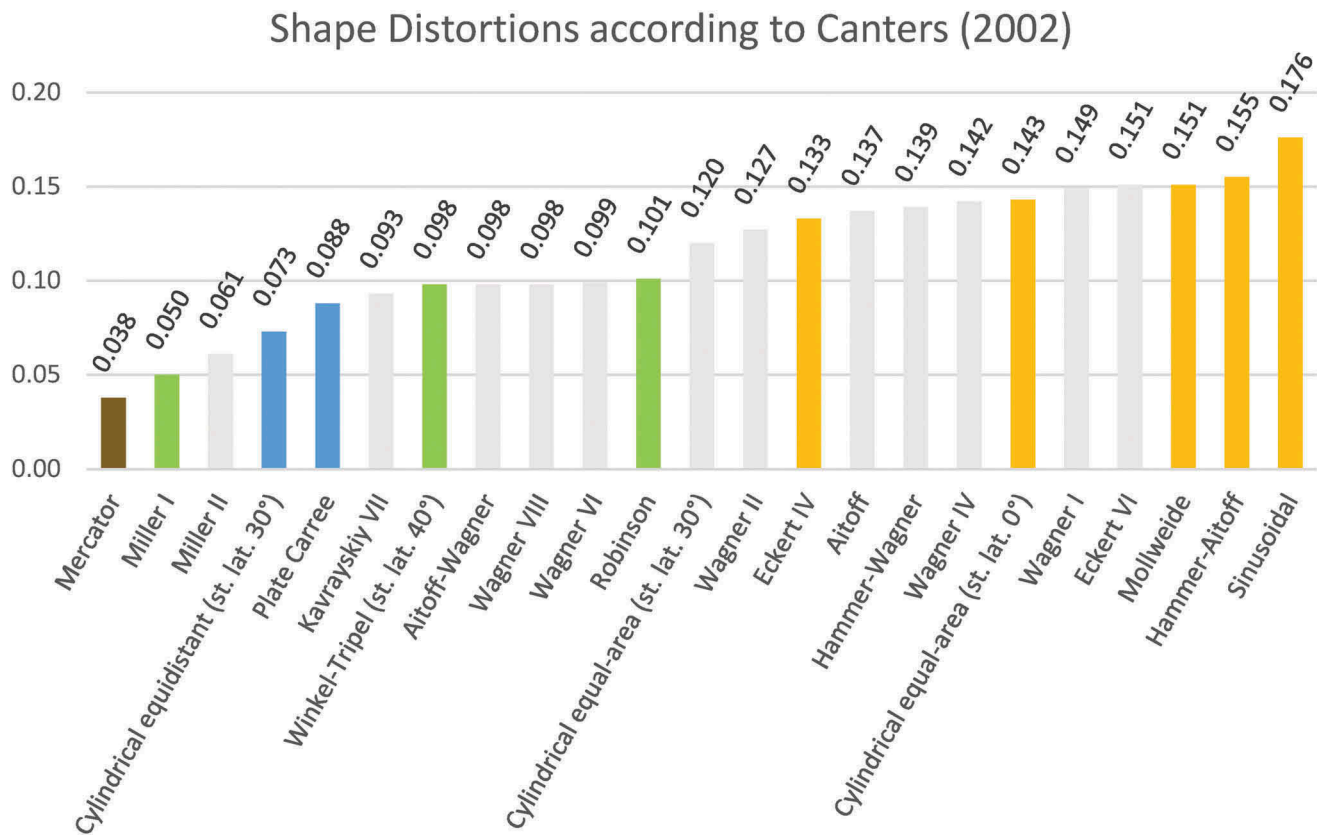


**Figure 6.** Mean shape distortion values of the world map projections tested by Canters (2002). Gray colors show the projections that are not available in our study.

as can be seen from the maps in Appendices I, II, IV, and V as well as the appearances and indicators of the sample landmasses given in Appendices III and VI. This shows that the elongation distortion indicator is more sensitive to the shape distortion than the compactness distortion indicator in most cases.

The general order of the projections from the lowest to the highest distortion became Mercator, Compromise, Equidistant, and Equal-Area according to the compactness distortion indicator and Compromise/Mercator, Equidistant, and Equal-Area according to the elongation distortion indicator. These findings also support the effectiveness of the indicators in measuring shape distortion. Among the Compromise projections, Times exhibited the best overall performance. An interesting finding was that Bonne had lower mean elongation distortion than the Equidistant and some of the Compromise projections although it is an equal-area projection, in which shape deformation is expected to be high. This is because its distortion pattern is centered on the northern hemisphere where most landmasses are located.

The level of detail influenced the values of the mean distortion indicators differently in most cases. In this context, the compactness distortion indicator caused higher

difference than the elongation distortion indicator. This mainly stems from scale-induced change at the level of detail of the datasets. To be specific, generalization dramatically decreases the perimeter of the landmasses with very irregular boundaries while the variation in the area becomes relatively less. Therefore, the compactness distortion indicator values of the landmasses such as Canada, Greenland, and Russia are affected more from the variation at the level of detail. On the other hand, the differences are small for most of the countries. Consequently, the results obtained from 1:50 M scale can be assumed to be valid for the scale range in which world maps are made concerning the elongation distortion indicator while they should be deemed valid for the scales around 1:50 M for the compactness distortion indicator.

Compared to the findings of Canters (2002), given in Figure 6, the compactness distortion indicator showed a great similarity while the elongation distortion indicator had significant discrepancies. In terms of the compactness distortion, the only significant difference appeared in the equidistant projections, which produced lower distortions in the Canters' study. Concerning the elongation distortion, the only significant similarity was that Mercator and Miller Cylindrical produced low distortion in both studies.



Furthermore, Canters' approach yielded mean values in a similar range with the compactness distortion indicator. Although Boyce and Clark's method used by Canters (2002) measures compactness in a different way, the differences with the compactness distortion indicator possibly stem from the reasons explained in Section 1.1. Besides, a few projections tested by Canters use different parameters compared to the same projections employed in this study.

## 7. Conclusions

In this article, we have introduced new measures for world map projections to evaluate them in terms of shape distortion. Apart from the previous studies, this has been the first study that both offers new distortion indicators about compactness and elongation valid at finite scale and takes into account the fiat and bona fide boundaries of the landmasses directly.

The planar and spherical compactness measures were basically developed through the area and perimeter of the landmass polygons. The planar and spherical elongation measures were principally developed by means of the lengths of the parallel and meridian line sections within the landmass polygons. The distortions were obtained from the ratio of the planar and spherical measure values. The distortion indicators were then computed by standardizing the distortion values.

The continental and country-specific shape distortion analyses were carried out for 16 sphere-based world map projections using the compactness and elongation distortion indicators. The elongation distortion indicator was found to be more sensitive to the shape distortion than the compactness distortion indicator in general. The results were not fully consistent between the indicators. However, for both indicators, Mercator and the compromise projections usually produced the lowest shape distortion followed by the equidistant and the equal-area projections in the ascending order.

The effect of the level of detail became very low for the elongation distortion indicator while it was more apparent for the compactness distortion indicator. The correlations between the indicators were moderate or high depending on the map projection.

The proposed approach is quite practical and can easily be performed in any GIS or cartographic environment that supports sphere-based world map projections. The findings can contribute to both map makers and map users. Map makers can benefit from them when designing world maps while map users can gain more awareness in this respect.

In future works, different kinds of shape distortion measures can be developed and an optimum approach can be identified for their integration. Besides, other

world map projections can also be analyzed from the shape distortion aspect. Furthermore, the area distortion measure can be integrated with shape distortion measures to evaluate compromise world map projections in both aspects. Another interesting study can be to investigate the perceptual performance of shape distortion measures based on user surveys.

## Acknowledgments

The authors would like to thank the editor and anonymous reviewers for their helpful and constructive comments that greatly contributed to improving the manuscript.

## Disclosure statement

No potential conflict of interest was reported by the authors.

## ORCID

Melih Basaraner  <http://orcid.org/0000-0002-4619-7801>

Sinan Cetinkaya  <http://orcid.org/0000-0002-3133-6514>

## References

- Angel, S., Parent, J., & Civco, D. L. (2010). Ten compactness properties of circles: Measuring shape in geography. *The Canadian Geographer/Le Geographe Canadien*, 54, 441–461. doi:10.1111/j.1541-0064.2009.00304.x
- Basaraner, M., & Cetinkaya, S. (2017). Performance of shape indices and classification schemes for characterising perceptual shape complexity of building footprints in GIS. *International Journal of Geographical Information Science*, 31, 1952–1977. doi:10.1080/13658816.2017.1346257
- Boyce, R. R., & Clark, W. A. (1964). The concept of shape in geography. *The Geographical Review*, 54, 561–572. doi:10.2307/212982
- Brainerd, J., & Pang, A. (2001). Interactive map projections and distortion. *Computers and Geosciences*, 27, 299–314. doi:10.1016/S0098-3004(00)00108-4
- Canters, F. (2002). *Small-scale map projection design*. London: Taylor & Francis.
- Canters, F., Deknopper, R., & De Genst, W. (2005). A new approach for designing orthographic world maps. *Proceedings of the 22nd International Cartographic Conference*. Spain: A Coruna.
- Costa, L. F., & Cesar, R. M. (2009). *Shape classification and analysis: Theory and practice* (2nd ed.). Boca Raton, FL: CRC Press.
- ESRI (2004). *Understanding map projections*. Redlands, CA: ESRI.
- Goldberg, D., & Gott, J. R. (2007). Flexion and skewness in map projections of the earth. *Cartographica*, 42, 297–318. doi:10.3138/carto.42.4.297
- Jenny, B., Savric, B., Arnold, N. D., Marston, B. E., & Preppernau, C. A. (2017). A guide to selecting map projections for world and hemisphere maps. In M. Lapaine & E. L. Usery (Eds.), *Choosing a map projection* (pp. 15–48). Cham, Switzerland: Springer.

- Kimerling, J. A., Overton, S. W., & White, D. (1995). Statistical comparison of map projection distortions within irregular areas. *Cartography and Geographic Information Systems*, 22, 205–221. doi:[10.1559/152304095782540348](https://doi.org/10.1559/152304095782540348)
- Laskowski, P. (1997). Part 1: Distortion-spectrum fundamentals: A new tool for analyzing and visualizing map distortions. *Cartographica*, 34(3), monograph 50, 3–18. doi:[10.3138/Y51X-1590-PV21-136G](https://doi.org/10.3138/Y51X-1590-PV21-136G)
- MacEachren, A. (1985). Compactness of geographic shape: Comparison and evaluation of measures. *Geografiska Annaler: Series B, Human Geography*, 67, 53–67. doi:[10.1080/04353684.1985.11879515](https://doi.org/10.1080/04353684.1985.11879515)
- Maling, D. H. (1992). *Coordinate systems and map projections* (2nd ed.). Oxford: Pergamon Press.
- Mulcahy, K. A., & Clarke, K. C. (2001). Symbolization of map projection distortion: A review. *Cartography and Geographic Information Science*, 28, 167–181. doi:[10.1559/152304001782153044](https://doi.org/10.1559/152304001782153044)
- Natural Earth – Cultural Vectors – 1:10 m – 1:50 m – 1:110 m. Retrieved from <http://www.naturalearthdata.com/downloads/>
- Neal, F. B., & Russ, J. C. (2012). *Measuring shape*. Boca Raton, FL: CRC Press.
- Ram, B. (2012). *Engineering mathematics, volume II*, (2nd ed.). Delhi: Pearson.
- Robinson, A. H., & The Committee on Map Projections. (2017). Choosing a world map: Attributes, distortions, classes, aspects. In M. Lapaine & E. L. Usery (Eds.), *Choosing a map projection* (pp. 15–48). Cham, Switzerland: Springer.
- Savric, B., Jenny, B., Patterson, T., Petrovic, D., & Hurni, L. (2011). A polynomial equation for the natural earth projection. *Cartography and Geographic Information Science*, 38, 363–372. doi:[10.1559/15230406384363](https://doi.org/10.1559/15230406384363)
- Savric, B., Jenny, B., White, D., & Strebe, D. R. (2015). User preferences for world map projections. *Cartography and Geographic Information Science*, 42, 398–409. doi:[10.1080/15230406.2015.1014425](https://doi.org/10.1080/15230406.2015.1014425)
- Snyder, J. P. (1987). *Map projections: A working manual*. USGS Professional Paper 1395. Washington, DC: United States Government Printing Office.
- UCLA Geoportal - Data Sets - World Continents. Retrieved from [http://gis.ucla.edu/geodata/dataset/continent\\_ln](http://gis.ucla.edu/geodata/dataset/continent_ln)
- Wentz, E. (1997). Shape analysis in GIS. *Proceedings of Auto-Carto 13*, Seattle (pp. 204–213). Retrieved from <https://cartogis.org/docs/proceedings/archive/auto-carto-13/pdf/shape-analysis-hi-gis.pdf>